Optimal Process Conditions for Powder Bed Fusion and Analysis of Properties of Maraging Steel

A Ra Jo[1,2] · Ji Seob An[1,2] · Sun Hyung Kim[1] · Dong Yong Park[1] · Young Hoon Moon[2] · Sun Kwang Hwang[1]

Abstract

Powder bed fusion (PBF), an additive manufacturing technology, has been widely used in the manufacturing field to create complex designs. Most PBF process studies have investigated the effect of laser power and scan speed on the mechanical properties and porosity of microstructure. In this study, five process conditions were selected to obtain superior properties of maraging steel, which were validated by absolute density analysis, hardness, and tensile tests. Maraging steel exhibits diverse mechanical properties depending on the heat-treatment combinations of solution annealing and aging. Mechanical property tests were conducted to compare the various temperature properties of the fabricated maraging steel under optimal conditions. Maraging steel exhibited a hardness of 612.7 HV and a tensile strength of 1925.6 MPa at 25 °C, and the strength was greater than 1000 MPa at temperatures below 600 °C. Additionally, the applicability of a fabricated die for maraging steel was investigated. The maraging steel die and American Iron and Steel Institute (AISI) D2 were analyzed by a forging process based on die load data sensing with a piezoelectric bolt. The maximum loads of the sensor in horizontal and vertical directions were 24.7% and 15.8% lower for the fabricated die than those of AISI D2. The findings confirm that the fabricated maraging steel is a suitable manufacturing process for commercial processes and can be used to manufacture dies with complex shapes.

Keywords Process condition · Maraging steel · Powder bed fusion · Additive manufacturing · Data sensing

1 Introduction

In general, subtractive manufacturing is commonly used in the manufacturing of products. However, this process yields a low material recovery rate and imposes restrictions on the product shape. Compared with the conventional forming process, mass production is difficult. Various alternative technologies are being employed to replace the processes involved in subtractive manufacturing. Among these alternative technologies, additive manufacturing (AM) enables the manufacturing of complex geometries by reducing material waste in various application fields, such as automobiles, medicine, and aerospace [1, 2]. Powder bed fusion (PBF) is an AM process that selectively scans the powder bed and melted powder to fabricate the product layer-by-layer, as illustrated in Fig. 1 [3, 4]. According to the shape designed by the user, the powder is fabricated to obtain the desired shape. Kuo et al. [5] and Kuo, and Qiu [6] conducted studies on manufacturing an injection mold with a complex cooling channel using the direct metal laser sintering method, one of the PBF technologies. These studies confirmed that the PBF process can be useful for fabricating mold systems with complex geometries.

In particular, PBF can produce products with various mechanical properties depending on the process conditions. Sendino et al. [7] compared and analyzed the correlation of product surface roughness with particle size distribution. Park et al. [8] investigated the effect of laser power and scan speed in controlling process conditions and compared the pore distribution. As the scan speed increased, many pores were created inside the material

A Ra Jo and Ji Seob An have contributed to the work equally and should be regarded as co-first authors.

✉ Sun Kwang Hwang
skhwang@kitech.re.kr

[1] Smart Manufacturing Technology R&D Group, Korea Institute of Industrial Technology, Daegu 42994, Republic of Korea

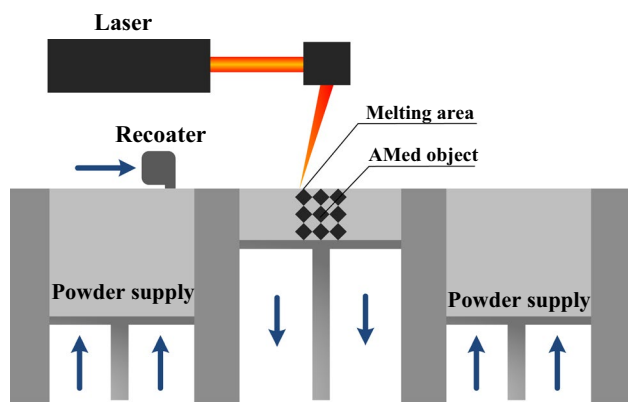[2] Department of Mechanical Engineering, Pusan National University, Busan 46241, Republic of Korea

Fig. 1 Schematic diagram of PBF

and the pores did not affect strain hardening. Benoit et al. [9] compared the process results by controlling the process conditions according to power, scan speed, and nominal energy density and checking or porosity and cracks in the microstructure. The shape and characteristics of pores depend on the laser scan speed, with irregular pores due to lack of fusion occuring at high scan rates and large pores observed at slow scan rates. Badrossamay et al. [10] studied the process condition consequences by comparing layer thickness, scan speed, power, and relative density and observing the microstructure. The use of a thicker powder layer was found to result in a larger melt pool and slower cooling rate, which greatly affects the microstructure. Vaudreuil et al. [11] compared mechanical properties according to the correlation between power and scan speed when thick layers were used. A microstructure with excellent mechanical properties was obtained by considering the optimal power and scan speed. In most previous studies, the laser power and scan speed of process conditions have been mainly explored. However, as these processes were limited in their ability to obtain superior properties, additional process parameters and analysis methods must be considered.

Maraging steel is frequently used in dies because of its weldability and high strength [12, 13]. As reported by Mooney et al. [14], maraging steel manifests various mechanical properties depending on the heat-treatment conditions. In this context, martensite, which is generated during aging and cooling conditions, increases the strength of the maraging steel. According to the American Society for Metals (ASM) Handbook [15], the mechanical properties of maraging steel exhibit fewer variations depending on the building direction (BD) compared with those of other fabricated materials. Based on these characteristics, maraging steel can serve as an appropriate die material to replace American Iron and Steel Institute (AISI) D2 and AISI H13, which are typically used as dies [16].

Generally, die life cannot be easily predicted because the die condition cannot be accurately determined in real time. Kim et al. [17] acquired data by installing a piezobolt sensor to inspect problems associated with the forging process. The sensor was used to gather data regarding the load applied to the die during the forging process. Based on the received data, the load applied to the die was measured during the forging process. They considered that the analysis of dies was possible through data sensing using piezoelectric bolts. Jang et al. [18] established a monitoring system for a laboratory-scale cup drawing process through a bolt-type piezoelectric sensor. A system for real-time monitoring of formability was developed to quantitatively analyze the time series data of the measured load. The measured load data showed a specific pattern, and they predicted forming quality in real time to prevent defects of cup drawing specimen.

In this study, we selected the PBF process conditions to improve the properties of the products compared with those of bulk materials. To obtain excellent properties, the laser power, scan speed, hatching distance, hatching angle, and layer thickness were considered as the process parameters. Moreover, the process conditions were selected based on absolute density, hardness, and tensile tests. After heat-treatment under various conditions, the optimal condition was selected based on the hardness tests, tensile tests, and microstructures. The high-temperature tensile properties of the selected specimens were analyzed for each BD. Furthermore, a finite element analysis (FEA) was performed to design a die with a simple shape. Following data sensing using a piezoelectric bolt, the designed die was compared and analyzed with maraging steel and an AISI D2 die. The fabricated maraging steel die was checked for the its applicability in the forming industry.

2 Experimental

2.1 PBF Fabrication

Maraging steel is primarily used in various industrial components, and in this study, it was used in a powder form for fabrication. The chemical compositions of the powder are listed in Table 1. Fig. 2a shows the fabrication equipment (ProX DMP 320, 3D systems, Rock Hill, USA) used; the diameter of the recommended powder was 30–100 μm. However, the variables may exhibit unexpected variations owing to nonuniform particle sizes. Therefore, the particle size of the powder was analyzed using a Mastersizer3000 (MAZ5222, Malvern, Worcester, United Kingdom)[19].

This study considered a wide range of five parameters to obtain desirable properties (Table 2). The absolute density was determined using a gas pycnometer (AccuPyc II 1340, Micromeritics, Atlanta, USA) for selecting the fabrication

Table 1 Chemical composition of maraging steel

Element	Fe	Co	Ti	Ni	Mo	Cr	S	P	Mn	Si	C
Maraging steel	Remainder	8.5–10	0.8–12	17–19	4.5–5.2	≤0.25	≤0.01	≤0.01	≤0.15	≤0.10	≤0.03

(a) **(b)**
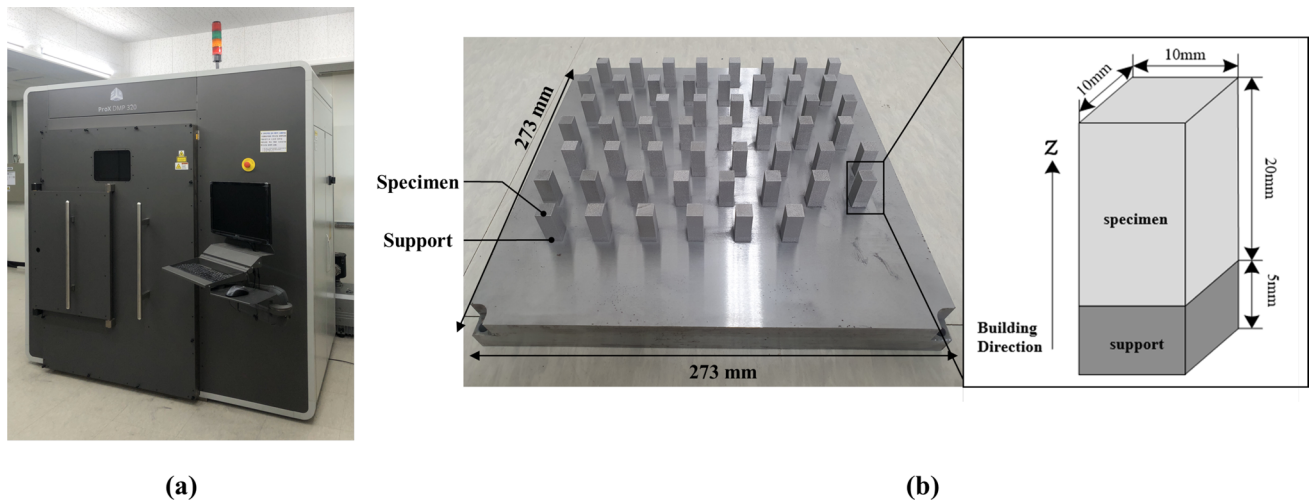
Fig. 2 **a** Fabrication equipment (DMP 320) and **b** specimens fabricated for selection of process conditions

Table 2 Range of condition parameters

Process conditions	Laser power (W)	Scan speed (mm/s)	Hatching angle (°)	Layer thickness (µm)	Hatching distance (µm)
Range	205–500	315–1500	15–355	30, 60	60–150

process conditions, and the bulk materials were compared. Conventionally, the PBF process uses energy density to derive the average applied energy per volume of material, and the energy density is formulated in Eq. (1) [20, 21]. The energy density and absolute density were compared to consider all the parameters and determine the correlation between them. In total, 219 specimens were fabricated with various parameters, and the specimen dimensions were 10 mm × 10 mm × 20 mm, as depicted in Fig. 2b. The relationship between the absolute density and energy density of all specimens was investigated, and the three most suitable conditions were selected.

$$\frac{\text{Laser power (W)}}{\text{Scan speed(mm/s)} \times \text{Hatching distance}(\mu m) \times \text{Layer thickness}(\mu m)}$$
$$= \text{Energy density(J/mm}^3)$$

(1)

Hardness and tensile tests were conducted on the specimens to select the best among the three previously selected process conditions, and the three specimens were compared

to bulk materials. The specimens used for the hardness and tensile tests were fabricated according to BD (horizontal and vertical), as illustrated in Fig. 3a. The hardness test was performed using a micro-Vickers hardness tester (VH3300, Buehler, Lake Bluff, USA) according to the American Society for Testing and Materials (ASTM) standard [22]. To obtain the ultimate tensile strength (UTS) and elongation, the tensile test was performed using a universal testing machine (ACEONE, Inchon, Korea) and a digital image correlation (DIC) camera for digital extensometer (ARAMIS SRX, Carl Zeiss GOM, Braunschweig, Germany) with a strain rate of 0.01/s. The tensile test specimen according to the ASTM standard [23] is shown in Fig. 3b.

2.2 Heat-Treatment Characterization and High-Temperature Tensile Properties

Maraging steel can exhibit various strength properties depending on the heat-treatment conditions. In this study, the heat-treatment method introduced by Bai et al. [24] and Lee et al. [25] was employed. They developed a heat-treatment method for solution annealing and aging using bulk maraging steel (Table 3). The temperatures of solution annealing and aging were 815 ℃ and 480 ℃, respectively. The specimens for heat-treatment were prepared according to the most suitable process conditions in a previous experiment and BD. The heat-treatment experiment was conducted in an argon atmosphere to prevent
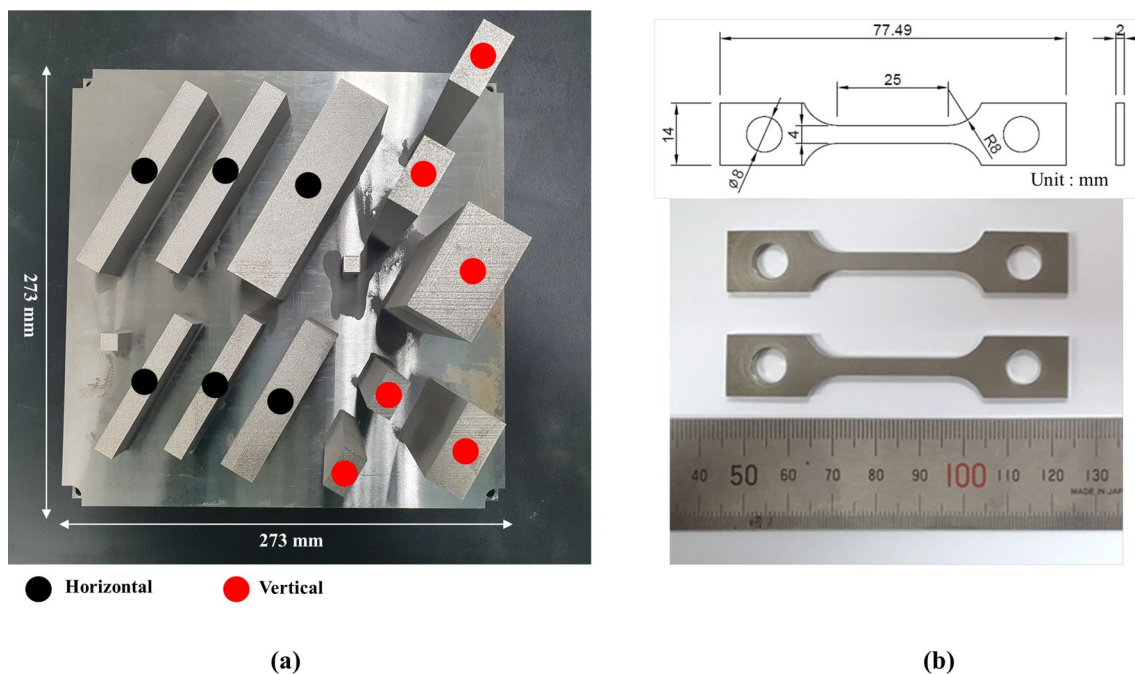
Fig. 3 **a** Tensile specimens based on the BD and **b** shape of tensile test specimen

Table 3 Heat-treatment conditions

Condition	Solution annealing (815 °C)	Aging (480 °C)
a	–	–
b	1 h	–
c	–	2.5 h
d	1 h	2.5 h

oxidation, followed by air cooling. After heat treatment, the hardness tests, tensile tests, and microstructure analyses were performed on maraging steels with various strengths depending on the heat-treatment conditions to determine the optimal method with the highest strength. The hardness test was conducted 10 times with a micro-Vickers hardness tester, and the tensile test was conducted with the same universal testing machine and DIC camera for digital extensometer with a strain rate of 0.01 /s. The microstructures were analyzed to measure the variation in martensite according to the heat-treatment conditions and were compared with the bulk and fabricated materials based on electron backscatter diffraction (EBSD) (JSM-7900F, JEOL, Tokyo, Japan).

A high-temperature tensile test was conducted to analyze the high-temperature tensile properties of maraging steel. The optimal process and heat-treatment conditions were used to fabricate the specimens, which were then put through a series of temperature tests. The form of the high tensile test specimen is shown in Fig. 4a. In addition, high-temperature tensile tests were conducted using Gleeble (3800-GTC, Dynamic Systems Inc., New York, USA) according to the ASTM standard [26], as depicted in Fig. 4b. The test temperatures were 400, 500, 600, 700, and 800 °C, and the test speed was 0.01/s.

2.3 Die Applicability

To confirm the applicability of the fabricated die to maraging steel, the fabricated die and the AISI D2 die were compared in terms of data sensing. The die was designed in a simple forging shape, as shown in Fig. 5a, and analyzed using DEFORM-2D (10.0, Scientific Forming Technologies Corporation, Ohio, USA). During the forging process, two piezoelectric bolts (Fig. 5b) were used to apply vertical and horizontal loads on the die. Repeated experiments were performed with a forging process that involved a speed of 0.2 mm/s with a stroke length of 2 mm. The specimen material used in the experiment was AISI 1045, and the experimental setup using a universal testing machine (ACEONE, Inchon, Korea) is presented in Fig. 5c.
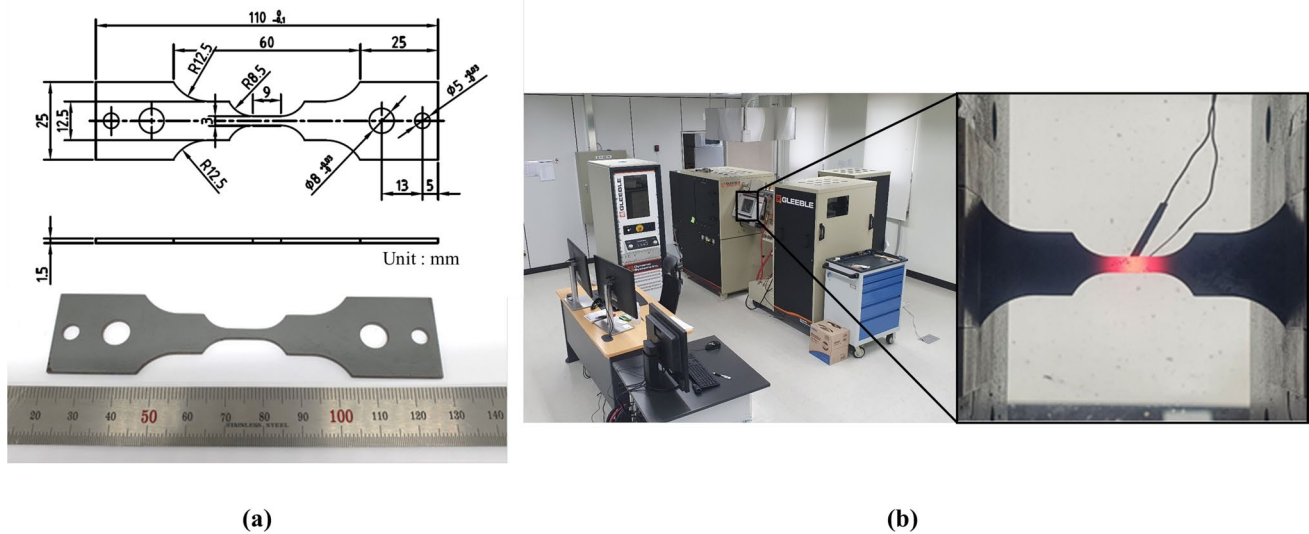
Fig. 4 **a** High-temperature tensile test specimens and **b** setup of high-temperature tensile test using Gleeble
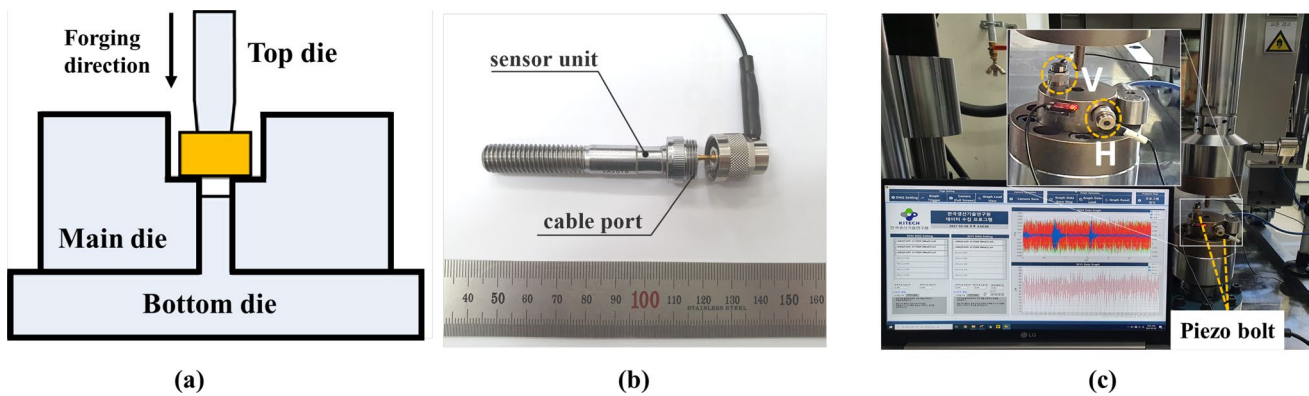

Fig. 5 **a** Schematic of the forging process setup, **b** Piezo Bolt for data sensing, and **c** sensor mounted on test equipment

3 Results and Discussion

As depicted in the powder diameter distribution graph in Fig. 6a, the diameter ranged from 20 to 70 μm, with the majority spanning within 30–50 μm having an average diameter of 40.9 μm. The size distribution was predominantly uniform and reasonably satisfied the value recommended by the equipment. Therefore, the fabricated powder was deemed appropriate for use in fabrication.

The specimens were manufactured under 219 conditions, considering the variables of laser power, scan speed, hatching angle, laser thickness, and hatching distance. In this paper, 219 manufacturing conditions and absolute density measurements were the most time consuming and difficult. In order to overcome these limitations, it is necessary to apply methods such as various optimization and test design methods. The absolute density and energy density of all specimens were measured and evaluated, and the results are depicted in Table 4 and Fig. 6b. As the energy density increased, the absolute density also tended to increase but converged above a certain value. Furthermore, if the energy density was exceedingly low or certain process conditions were inaccurate, the specimens underwent swelling and fell because of poor fabrication, as depicted in Fig. 6b. Among these conditions, three representative conditions for the theoretical density of 8.1 g/cm^3 of maraging steel were selected. The three selected conditions are listed in Table 5. Gas pycnometry is the most reliable non-destructive method for absolute density measurement. It was confirmed that absolute density measurement method is simple and reasonable compared to the pore check of the specimen surface which is a general method for finding the optimal
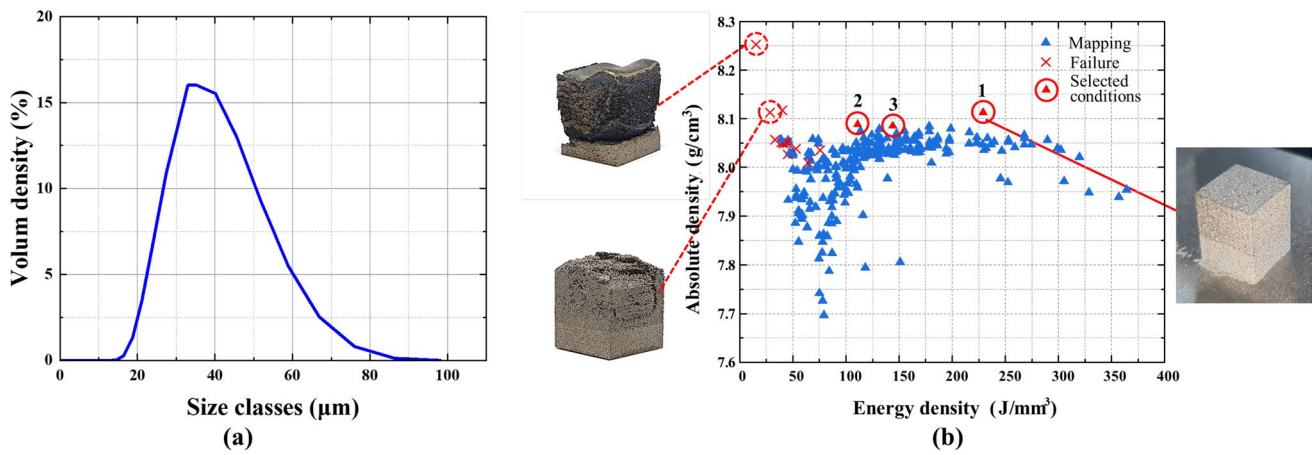
Fig. 6 **a** Distribution of maraging steel powder and **b** variation of absolute density with energy density with images of failure specimens

Table 4 AM conditions listed in descending order of absolute density

Condition No	Laser power (W)	Scan speed (mm/s)	Hatching angle (°)	Layer thickness (µm)	Hatching distance (µm)	Absolute density (g/cm³)	Energy density (j/mm³)
21	330	505	350	30	95	8.1123	229.29
2	295	1180	120	30	75	8.0880	111.11
3	300	925	130	30	75	8.0847	144.14
4	450	700	90	30	120	8.0842	178.57
5	330	615	264	30	90	8.0799	198.74
6	450	950	45	30	120	8.0782	131.58
7	420	695	355	30	130	8.0747	154.95
8	300	440	265	60	100	8.0745	113.64
9	350	660	85	30	130	8.0737	135.98
10	450	700	45	30	120	8.0736	178.57
⋮			⋮				⋮
214	215	315	75	60	135	7.7874	84.26
215	325	315	311	30	110	7.7669	312.65
216	440	1305	145	30	150	7.7419	74.93
217	470	1335	310	30	150	7.7268	78.24
218	500	1500	180	30	140	7.6970	79.37
219	405	1100	115	60	75	7.0071	81.82

Table 5 Three process conditions selected by density measurements

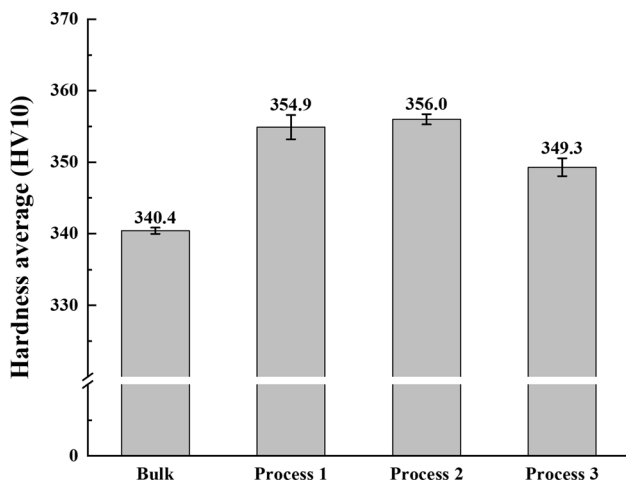| Condition No	Laser power (W)	Scan speed (mm/s)	Hatching angle (°)	Layer thickness (µm)	Hatching distance (µm)	Absolute density (g/cm³)	Energy density (j/mm³)
1	330	505	350	30	95	8.1123	229.29
2	295	1180	120	30	75	8.0880	111.11
3	300	925	130	30	75	8.0847	144.14

Fig. 7 Vickers hardness average value according to process conditions

process for AM process. Evidently, Process 2 yields the lowest energy density among the three selected process conditions. It was concluded that the lowest energy

density, similar to the theoretical density, could be a suitable condition for energy efficiency in AM.

The hardness test results for the three selected processes are presented in Fig. 7. All three processes yielded slightly higher values than those of the bulk specimen. Process 2 yielded the highest value at 356.0 HV. The results of the tensile tests are presented in Fig. 8, wherein the horizontal and vertical BD results are shown in Fig. 8a and b, respectively. The elasticity modulus, UTS, and elongation results are summarized in Table 6. The bulk material showed 170 GPa of elasticity modulus, 1148.6 MPa of UTS, and 11.59% of elongation to fracture. Compared with the bulk material, both offered excellent properties, such as strength and elongation. Process 1 offered the highest UTS (1213.1 MPa) in the horizontal properties, but it exhibited the lowest elongation (8.95%) in the vertical properties. Process 2 offered the highest elasticity modulus (130 GPa) and elongation (12.43%) with comparable UTS value (1207.0 MPa) among the three process conditions. Finally, Process 3 yielded the lowest UTS (1092.8 MPa) and showed variations depending on the BD. According to Vaudreuil et al. [11], the modulus of elasticity, tensile strength, and deformation at break
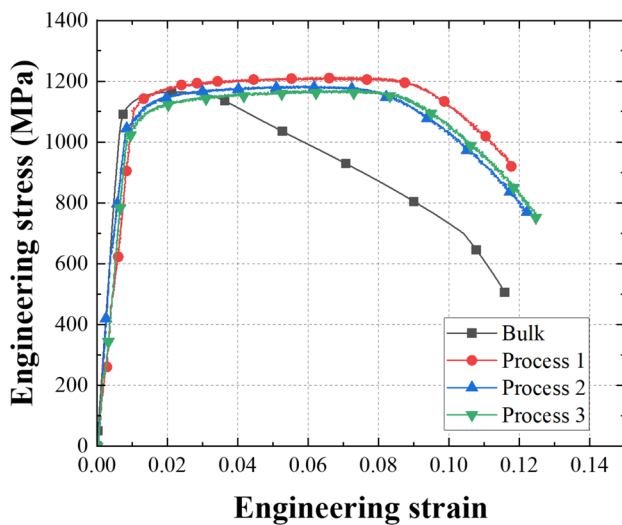
(a)
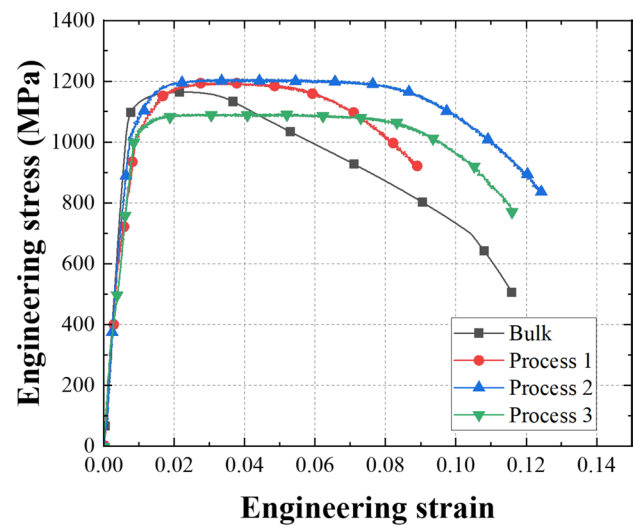
(b)

Fig. 8 Engineering stress–strain curves: **a** horizontal and **b** vertical building directions

Table 6 Tensile test results according to process conditions

Process No	Elasticity modulus (GPa)		UTS (MPa)		Elongation to fracture (%)	
	Horizontal	Vertical	Horizontal	Vertical	Horizontal	Vertical
Bulk	170		1148.6		11.59	
1	106	115	1213.1	1195.0	11.78	8.95
2	130	138	1184.5	1207.0	12.23	12.43
3	123	112	1169.5	1092.8	12.48	11.65

vary depending on the scan speed and laser power. From the results, the AMed maraging steel showed different mechanical properties owing to laser power, scan speed, hatching angle, and hatching distance. In future, the effect of the process conditions on the mechanical property of maraging steel such as elasticity modulus, strength, elongation can be studied. Therefore, we selected Process 2 as the optimal process with the lowest energy density and appropriate mechanical properties, which exhibits fewer variations depending on the BD compared with those of other processes.

The specimens fabricated under the conditions adopted from the previous test were heat-treated using the three methods listed in Table 3. To select the condition with the best mechanical properties among the three heat-treatment conditions, hardness and tensile tests were conducted, followed by microstructure analysis (Table 7).

The results of the hardness test on bulk and fabricated specimens are portrayed in Fig. 9a. Overall, the results showed similar tendencies, but the hardness values of the fabricated specimens were generally higher than those of the bulk specimens. This indicates that the fabricated material

can be used as a substitute for bulk products. Under heat-treatment conditions c and d, the hardness values of the fabricated material were 583.3 and 612.7 HV, respectively, which improved by approximately 163.8% and 172.1% compared to those measured prior to heat-treatment. From the results, condition d of the heat treatment showed the highest hardness value. With the addition of 6 h of aging time while conducting the experiment under heat-treatment condition d, the hardness diminished to 594.0 HV. This was confirmed by the reduced hardness as martensite reverted to ferrite and austenite [15]. The condition (815 ℃ with 1 h, 480 ℃ with 2.5 h) can be applied in die manufacturing.

The vertical and horizontal flow stress curves of the fabricated specimens are presented in Fig. 9b. The results for the bulk specimen were added and compared only for heat-treatment condition d. As revealed by the tensile test results, almost no vertical or horizontal differences existed under all conditions and the variation in strength was similar to the hardness measurement results. Similar to the hardness test results, it displayed the highest strength under heat-treatment condition d, and the strength of the fabricated specimen were

Table 7 Tensile test results according to heat-treatment conditions

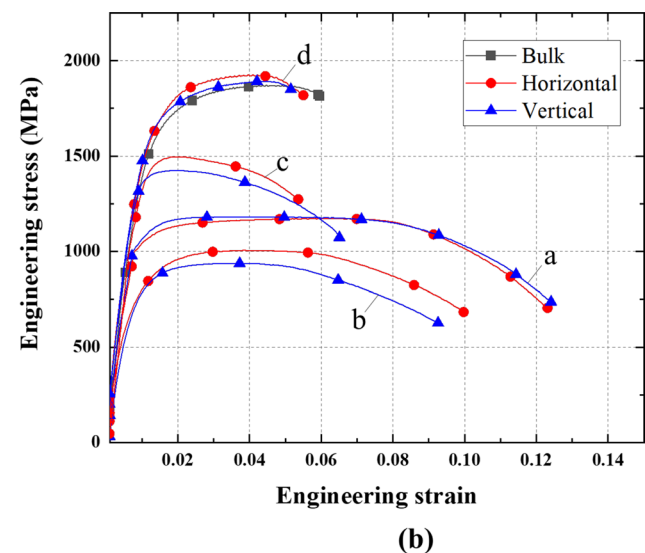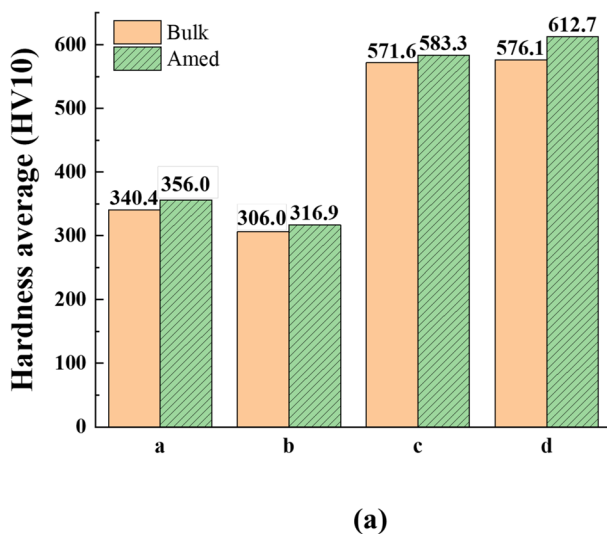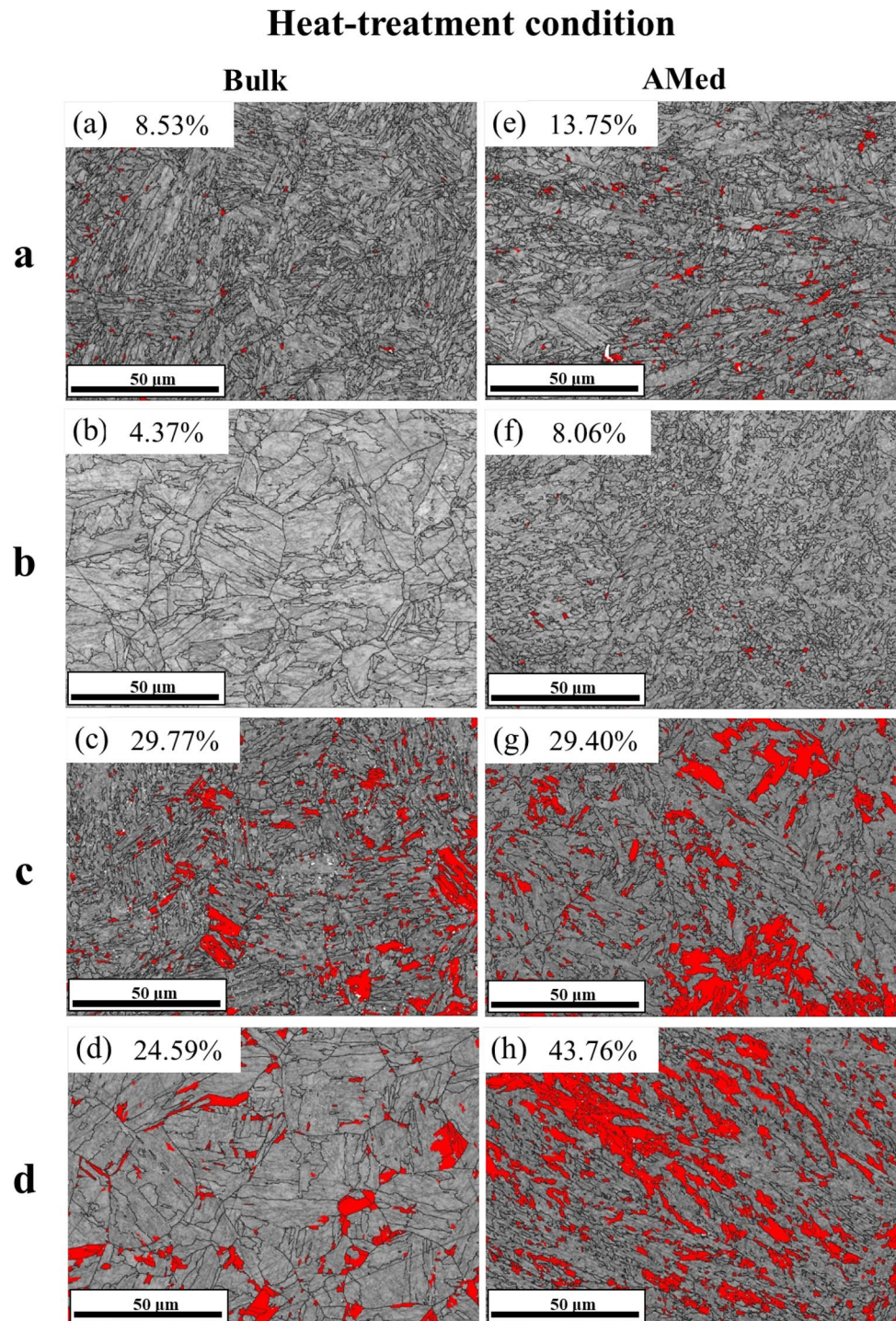| Condition	Elasticity modulus (GPa)		UTS (MPa)		Elongation to fracture (%)	
	Horizontal	Vertical	Horizontal	Vertical	Horizontal	Vertical
a	130	138	1184.5	1207.0	12.23	12.43
b	129	121	1007.1	938.0	9.97	9.26
c	162	160	1495.7	1425.0	5.36	6.51
d	163	160	1925.6	1889.6	5.50	4.16
d (Bulk)	163		1871.5		5.96	

Fig. 9 Post heat-treatment results of **a** Vickers hardness test and **b** tensile test

greater than condition a (no heat treatment). Based on the tensile test results, we confirmed that if heat-treatment condition d was applied, the UTS (1925.6 MPa) and elasticity modulus (163 GPa) of the specimen improved by 162.6% and 125.4% compared with those measured prior to heat treatment. Thus, the UTS value is significantly increased by additive solution annealing (815 °C with 1 h) compared with the case of only aging heat-treatment (condition c).

The analysis results of the martensite fraction of maraging steel based on the heat-treatment conditions through EBSD measurements are presented in Fig. 10. For microstructure analysis, the martensite fraction was classified based on the band contrast (BC) value suggested by Baek et al. [27] using the BC map. Generally, a higher fraction of martensite indicates greater hardness and strength. Based on the microstructure analysis, the martensite fraction of the

Fig. 10 Evolution of martensite: **a–d** bulk specimens according to heat-treatment conditions and **e–h** fabricated specimens according to heat-treatment conditions
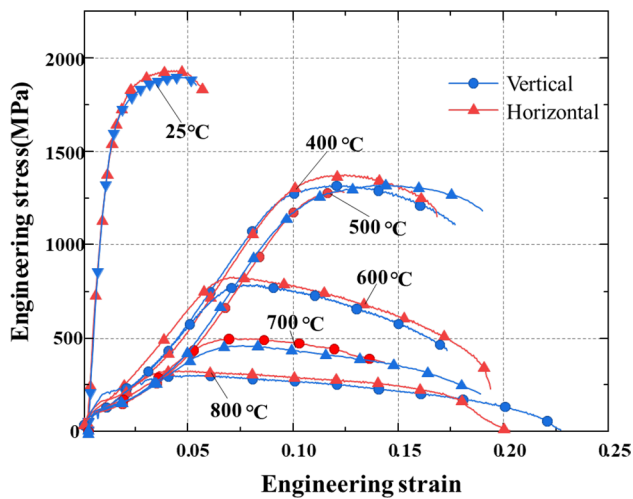
Fig. 11 Engineering stress–strain curves of high-temperature tensile test

Table 8 Tensile test results at high temperature

Temperature (°C)	UTS (MPa)		Elongation to fracture (%)	
	Horizontal	Vertical	Horizontal	Vertical
25	1925.6	1892.5	5.15	5.50
400	1374.4	1316.3	16.86	17.7
500	1288.0	1323.3	12.23	18.82
600	827.9	798.5	19.42	17.45
700	500.0	458.1	14.13	18.72
800	328.6	301.8	20.35	22.72

fabricated specimen was greater than that of the bulk specimen under all conditions. This is consistent with the hardness test results obtained earlier. Owing to the characteristics of the PBF process, heat is generated by the laser during processing, and martensite is generated during the cooling process. Based on the microstructure analysis results, we confirmed that the specimen under heat-treatment condition d exhibited the greatest strength and hardness, with a martensite fraction of 43.76%. Therefore, this heat-treatment condition was adopted based on the findings of the hardness test, tensile test, and microstructure analysis.

To examine the high-temperature tensile properties of maraging steel, we conducted tensile tests at high temperatures. The flow stress curves at 25 ℃ and 400–800 ℃ are presented in Fig. 11, and the UTS and elongation results according to temperature are listed in Table 8. Based on the high-temperature tensile test results, the vertical and horizontal tensile strengths and elongations at all temperatures remained almost constant. Therefore, the mechanical properties did not differ considerably depending on the fabrication direction. Generally, the temperature distribution of

the die used in the hot process is 200–500 °C [28–30]. In cases where the die temperature is less than 600 ℃, UTS of the hot-formed steel is estimated to be 1000 MPa or higher. In addition, compared with the physical properties of AISI H13, which is generally used in the hot process, the die fabricated under optimal fabrication conditions and heat-treatment can be used as hot-forming steel [31]. Based on the high-temperature tensile test results, we can predict that the fabricated maraging steel can be used as a die, designed with no vertical or horizontal strength aberrations and a free shape.

Based on the aforementioned results, a simple forging process was designed to examine the applicability of the fabricated maraging steel die, which was made under Process 2 condition and heat-treatment condition d. For the actual laboratory-scale experiment, the die shape and specimen size were designed according to the load of the testing equipment. Subsequently, we performed a die stress analysis using DEFORM-2D, as shown in Fig. 12a. The specimen shape was set at a diameter of 10 mm and a height of 4 mm. As shown in Fig. 5c, piezoelectric bolts were mounted to obtain load data in both vertical and horizontal directions, and the experiment was conducted under the conditions stated earlier. Under the same conditions, load was repeatedly applied to the die, as shown in Fig. 12b. The horizontal direction results presented in Fig. 12c indicate a positive value, whereas the vertical direction results presented in Fig. 12d exhibit a negative value. Thus, the tensile stress was generated horizontally, implying a positive value, and the compressive stress was generated in the vertical direction, denoting a negative value. Based on the load data, both maraging steel and AISI D2 exhibited a similar tendency, but a variation was observed between the maximum and minimum values. In the maraging steel die, the absolute value of the load was 35–191 N less than that of AISI D2 and that of the overall load was low. In particular, the maximum loads of piezoelectric bolts in horizontal and vertical directions were 24.7% and 15.8% lower than those of AISI D2. Predictively, maraging steel might have a longer die life compared to AISI D2 because a low load yields less die deformation. This experiment validated the applicability of the fabricated maraging steel dies even at 25 ℃. Therefore, the die made of AMed maraging steel is suitable for commercial products and can be manufactured with excellent mechanical properties even for complex shapes.

4 Conclusions

In this study, we derived optimal conditions for fabricating maraging steel using the PBF process. Heat-treatment conditions were proposed to improve the mechanical property of AM maraging steel. The die was designed and investigated
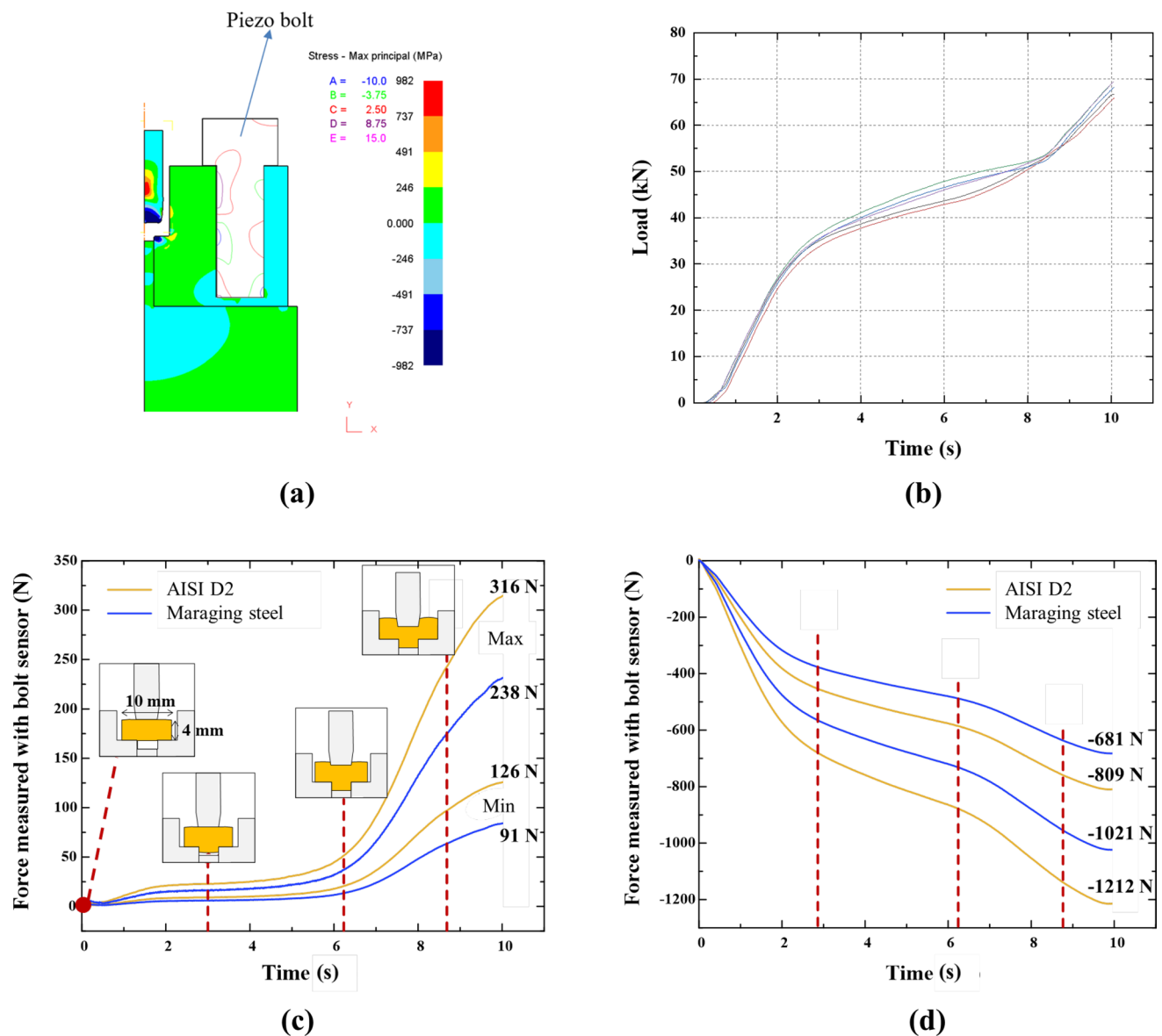
(a)

(b)

(c)

(d)

Fig. 12 **a** Forging die using FE analysis, **b** graph of load applied to the die and load variation in Piezo bolt according to forming **c** horizontal and **d** vertical

through forming load sensing to examine the applicability of the AMed maraging steel. The AMed maraging steel with PBF process can be applied in die industry for industrial application. The following detailed conclusions are drawn.

1. The optimal fabrication parameters were analyzed for the PBF process of maraging steel. In total, 219 processes—considering the laser power, scan speed, hatching angle, layer thickness, and hatching distance—were analyzed to determine the correlation between the absolute density and energy density. Among them, three processes that were representative of the ideal density of 8.1 g/cm^3 were selected.

2. Among the three process conditions, the optimal process was identified by conducting hardness and tensile tests in both horizontal and vertical directions, where Process 2 displayed the most suitable results with a hardness of 356.0 HV, a vertical UTS of 1207.0 MPa, and vertical elasticity modulus of 138 GPa. The optimal process conditions selected are as follows: laser power of 295 W, scan speed of 1180 mm/s, hatching angle of 120°, layer thickness of 30 μm, and hatching distance of 75 μm.

3. Heat treatment was proposed to improve the mechanical property of AMed maraging steel. The hardness and tensile tests and microstructure analysis results were compared under a combination of heat-treatment conditions:

solution annealing and aging. Based on the results, we confirmed that condition d (815 ℃ with 1 h, 480 ℃ with 2.5 h) yielded the highest strength (UTS 1925.6 MPa), hardness (612.7 HV), elasticity modulus (163 GPa), and martensite fraction (43.76%). In particular, at temperatures below 600 ℃, the strength was maintained at more than 1000 MPa, which was comparable to that of AISI H13.

4. To demonstrate the applicability of the fabricated maraging steel, a simple-shaped forging die was fabricated with maraging steel and compared with AISI D2. Piezoelectric bolts were used to acquire the vertical and horizontal direction loads applied to the die. The absolute value of the load was 35–191 N less than that of AISI D2 and that of the overall load was low. In particular, the maximum loads of piezoelectric bolts in horizontal and vertical directions were 24.7% and 15.8% lower than those of AISI D2. On the basis of these results, it was concluded that the die made of AMed maraging steel is suitable for commercial products and can be manufactured with excellent mechanical properties even in the case of complex shapes.

Declarations

Conflict of interest The authors report there are no competing interests to declare.

References

1. H.S. Yoon, J.Y. Lee, H.S. Kim, M.S. Kim, E.S. Kim, Y.J. Shin, W.S. Chu, S.H. Ahn, Int. J. Precis. Eng. Manuf. - Green Technol. **1**, 261–279 (2014). https://doi.org/10.1007/s40684-014-0033-0

2. M.Q. Zafar, H. Zhao, Met. Mater. Int. **26**, 564–585 (2020). https://doi.org/10.1007/s12540-019-00441-w

3. K. Kempen, L. Thijs, J. Van Humbeeck, J.-P. Kruth, Phys. Procedia **39**, 439–446 (2012). https://doi.org/10.1016/j.phpro.2012.10.059

4. M. Zhao, C. Duan, X. Luo, Met. Mater. Int. **28**, 2225–2238 (2022). https://doi.org/10.1007/s12540-021-01129-w

5. C.C. Kuo, Z.F. Jiang, X.Y. Yang, S.X. Chu, J.Q. Wu, Int. J. Adv. Manuf. Technol. **107**, 1223–1238 (2020). https://doi.org/10.1007/s00170-020-05114-2

6. C.C. Kuo, S.X. Qiu, Materials **14**, 7258 (2021). https://doi.org/10.3390/ma14237258

7. S. Sendino, S. Martinez, F. Lartategui, M. Gardon, A. Lamikiz, J.J. Gonzalez, Int. J. Adv. Manuf. Technol. **124**, 789–799 (2023). https://doi.org/10.1007/s00170-022-10423-9

8. S.H. Park, J.Y. Jang, Y.O. Noh, B.H. Bae, B.H. Rhee, D.R. Eo, J.W. Cho, Mechanical properties of 316L manufactured by selective laser melting (SLM) 3D printing, in *Proceedings of the Korean Society of Propulsion Engineers Conference* (The Korean Society of Propulsion Engineers, Daejeon, 2017), pp. 872–876. https://koreascience.kr/article/CFKO2017346625055423.page

9. M.J. Benoit, M. Mazur, M.A. Easton, M. Brandt, Int. J. Adv. Manuf. Technol. **114**, 915–927 (2021). https://doi.org/10.1007/s00170-021-06957-z

10. M. Badrossamay, A. Rezaei, E. Foroozmehr, A. Maleki, A. Foroozmehr, Int. J. Adv. Manuf. Technol. **118**, 1703–1717 (2022). https://doi.org/10.1007/s00170-021-07719-7

11. S. Vaudreuil, S.E. Bencaid, H.R. Vanaei, A. El Magri, Materials **15**, 8640 (2022). https://doi.org/10.3390/ma15238640

12. C.C. Kuo, Z.F. Jiang, Int. J. Adv. Manuf. Technol. **104**, 4169–4181 (2019). https://doi.org/10.1007/s00170-019-04198-9

13. S.W. Kim, H.W. Lee, Met. Mater. Int. **24**, 616–625 (2018). https://doi.org/10.1007/s12540-018-0078-7

14. B. Mooney, K.I. Kourousis, R. Raghavendra, Addit. Manuf. **25**, 19–31 (2019). https://doi.org/10.1016/j.addma.2018.10.032

15. ASM, Handbook Vol. 1: Properties and Selection: Irons, Steels, and High-Performance Alloys (ASM International, Materials Park,, 2005)

16. H. Coldwell, R. Woods, M. Paul, P. Koshy, R. Dewes, D. Aspinwall, J. Mater. Proces. Technol. **135**, 301–311 (2003). https://doi.org/10.1016/S0924-0136(02)00861-0

17. S.Y. Kim, A. Ebina, A. Sano, S. Kubota, Procedia Manuf. **15**, 542–549 (2018). https://doi.org/10.1016/j.promfg.2018.07.275

18. I. Jang, G. Bae, H. Kim, Mech. Syst. Signal Process. **180**, 109457 (2022). https://doi.org/10.1016/j.ymssp.2022.109457

19. G. Casalino, S.L. Campanelli, N. Contuzzi, A.D. Ludovico, Opt. Laser Technol. **65**, 151–158 (2015). https://doi.org/10.1016/j.optlastec.2014.07.021

20. A. Suzuki, R. Nishida, N. Takata, M. Kobashi, M. Kato, Addit. Manuf. **28**, 160–168 (2019). https://doi.org/10.1016/j.addma.2019.04.018

21. H. Gong, K. Rafi, H. Gu, T. Starr, B. Stucker, Addit. Manuf. **1–4**, 87–98 (2014). https://doi.org/10.1016/j.addma.2014.08.002

22. ASTM, Standard E92.82, Standard Test Method for Vickers Hardness of Metallic Materials (ASTM International, West Conshohocken, PA, 2006)

23. ASTM, Standard E28.04, E8M-04: Standard Test Methods for Tension Testing of Metallic Materials (ASTM International, West Conshohocken, PA, 2006)

24. Y. Bai, C. Zhao, J. Yang, R. Hong, C. Weng, H. Wang, J. Mater. Process. Technol. **288**, 116906 (2021). https://doi.org/10.1016/j.jmatprotec.2020.116906

25. D.G. Lee, K.C. Jang, J.M. Kuk, I.S. Kim, J. Mater. Process. Technol. **162–163**, 342–349 (2005). https://doi.org/10.1016/j.jmatprotec.2005.02.102

26. ASTM, Standard E21.09, Standard Test Methods for Elevated Temperature Tension Tests of Metallic Materials (ASTM International, West Conshohocken, PA, 2006)

27. M.S. Baek, K.S. Kim, T.W. Park, J.H. Ham, K.A. Lee, Mater. Sci. Eng. A **785**, 139375 (2020). https://doi.org/10.1016/j.msea.2020.139375

28. D.H. Kim, B.M. Kim, C.G. Kang, Finite Elem. Anal. Des. **41**, 1255–1269 (2005). https://doi.org/10.1016/j.finel.2004.11.005

29. M. Davoudi, A.F. Nejad, S.S.R. Koloor, M. Petrů, J. Mater. Res. Technol. **15**, 5221–5231 (2021). https://doi.org/10.1016/j.jmrt.2021.10.093
30. J. Ni, C.P. Cao, Y. Li, Procedia Manuf. **15**, 451–458 (2018). https://doi.org/10.1016/j.promfg.2018.07.252
31. D. Klobčar, J. Tušek, B. Taljat, Mater. Sci. Eng. A **472**, 198–207 (2008). https://doi.org/10.1016/j.msea.2007.03.025